Bilge International Journal of Science and Technology Research
ISSN: 2651-401X
e-ISSN: 2651-4028
Research Article
2022, Volume: 6, Issue: 2, 83-90
Received: 21.01.2022; Accepted: 22.03.2022
DOI: 10.30516/bilgesci.1060177

Tuning Optical and Electrical Properties of Ultra-Fast Prepared Nanoflower Mg:ZnO Films by MWCNTs Coating

Irmak Karaduman Er[1], Fatma Sarf[2*], Emin Yakar[3]

Abstract: Mg doped ZnO films were decorated by multi-walled carbon nanotubes (MWCNTs) *via* fast chemical bath onto ZnO seed layers. XRD analysis showed preferential orientation shift from high-energy (002) peak to low-energy (101) peak with MWCNTs coating. Average crystalline size of Mg doped ZnO samples were 15 nm. diameter and decreased by MWCNTs coating. SEM images revealed that the presence of accumulative nanoflower-rod forms on Mg:ZnO surfaces and net-shaped coating has been achieved by MWCNTs inclusion. No major difference was detected in optical absorption edge of both films however MWCNTs coating caused an increase direct band gap energy. Calculated band gap values were 3.04 eV and 3.34 eV in Mg:ZnO and Mg:ZnO/MWCNTs films, respectively due to Burstein-Moss effect. Electrical resistance results showed that MWCNTs decreased the resistance of films at room temperature which were calculated as 29.85 and 8.53 kΩ for Mg:ZnO and Mg:ZnO/MWCNTs films, respectively.

Keywords: Chemical bath deposition, ZnO, MWCNTs, electrical properties, optical properties.

[1]**Address:** Department of Medical Services and Techniques, Eldivan Medical Services Vocational School, Çankırı Karatekin University, Çankırı, Türkiye.

[2]**Address:** Çanakkale Onsekiz Mart University, Çan Vocational School, Çanakkale, Türkiye.

[3]**Address:** Department of Materials Science and Engineering, Faculty of Engineering, Çanakkale Onsekiz Mart University, Çanakkale, Türkiye.

***Corresponding author**: fatmaozutok@comu.edu.tr

Citation: Er Karaduman, I., Sarf, F., Yakar, E. (2022). Tuning Optical and Electrical Properties of Ultra-Fast Prepared Nanoflower Mg:ZnO Films by MWCNTs Coating. Bilge International Journal of Science and Technology Research, 6(2): 83-90.

1. INTRODUCTION

Opto-electronic device integration is so essential to produce Uv-photodedectors, CIGS-based solar modules, optical wave guides and LED screens. Chemical-mechanical stability and average crystallite size with shape of the particles have a big impact on the band gap tailoring that affect opto-electronic device performance. In the studies of GaN-replacement material, its useful optical properties are highlighted by its wide optical band gap energy (~3.37-3.82 eV), stimulated excitonic emission probability even above room temperature (RT) and high optical transperancy (>80%) in Uv-Vis region (Tan et.al., 2016; Kim et.al., 2013). The arrangement of the optical band gap energy with using ZnO is widely investigated by different research groups because localized surface defects have been created so recombination of electron-hole may be hindered (Samadi et.al., 2016).

ZnO nanostructures have shown remarkable properties that used in dye sensitized solar cells, pharmaceutical, photocatalysis and room temperature gas sensors (Yao et.al., 2014; Majunder et.al., 2020). The main advantages of ZnO nanostructures are supplying a direct pathway to conduction and transportation of electrons, large surface to volume ratio, creating active polar surfaces, reduce the mass transfer resistance and reduction interface effects (Yang et.al., 2012). VA group elements or transtion metal doping with/without IA/IIA group elements as well as carbon modification which including nanotubes, graphene, carbon fibers have been studied to achieve reproducible properties of the nanostructures (Okeke et.al., 2021). Alkaline earth metals can affect the physical and chemical character of ZnO. As a IIA group element, ionic radius of Mg^{2+} (0.57 Å) is so proper to replaceZn^{2+} ions (0.60 Å) so lattice stability can be ensured (Jaballah et.al., 2020). To obtain high mechanical

stability and functionality, multi-walled carbon nanotubes (MWCNTs) have been studied as a matrix form in nano-structures (Chen et.al., 2012). Functional groups on the surface of the walls can be helpful so physical and chemical properties of matrix structures can be improved.

Thin film production type is very important as being fast, simple and cheap in industrial applications. For this reason, chemical methods are preferred more than physical methods.There are many procedures involving the chemical reaction of precursors proposed and implemented by researcherssuch as hydrothermal, sputtering, atomic layer deposition and spin coating (Sharma et.al., 2015; Sahoo et.al., 2013; Papielarski et.al., 2019). Among them, chemical bath deposition is so attractive due to its easy production and set-up, ability of the storage of wastes. One characteristic of zinc is the tendency of zinc hydroxide to easily undergo dehydration reactions forming the oxide phase, which allows to obtain high ZnO crystal quality even in low-temperature production (Altun et.al, 2021).

Hence, an attempt was made to chemical bath deposition the Mg:ZnO nanoflower/MWCNTs matrix and evaluate its structural, electrical and optical properties in this study. Structural and morphological properties of ZnO seed layer were shown in our previous study (Sarf et.al., 2020).

2. MATERIAL AND METHODS

Mg doped and MWCNTs coated ZnO films were deposited by simple chemical bath onto ZnO nanoflower seed layers (1x4 cm). Nanoflower ZnO seed layer preparation procedure was explained in our previous study (Sarf et.al., 2020). All chemicals were purchased from Sigma Aldrich and used without any further purification. Zincacetate dihydrate ($Zn(Ac)_2.2H_2O$)(99%), magnesium acetate tehtrahydrate ($C_4H_6MgO_4$)(99%) and ammonium hydroxide (NH_4OH) were used as a zinc-source, Mg-source and complex agent, respectively. The total distilled water volume was 100 ml. and [Zn/Mg] molar ratio was arranged as [4/1]. Nanoflower ZnO seed layers were immersed into aqueous solution and pH of this solution was set to 11 with adding ammonia65±5 ºC and 8 min. were chosen as working temperature and working time for mixing the solution in the beaker on the hot plate. 10% metal containing MWCNTs (0.02 g) was added in aqueous solution to obtain Mg:ZnO/MWCNTs. After one day waiting, Mg:ZnO and Mg:ZnO/MWCNTs films were annealed at 450 ºC to remove surface residues.

The structural analysis of the films was performed by Rigaku SmartLab X-ray diffractometer at 1.5406 Å over 2θ range of 20º–80º. The surface morphology studies were carried out by JEOL JSM-7100F- SEM (scanning electron microscope). Chemical composition of the films was determined by FTIR (Fourier Transform Infrared Spectrum) monitoring VERTEX 70 with an attenuated total reflectance (ATR) Bruker, Germany. I-V measurements were carried out by using a computer-controlled system which was included Keithley 2400 source meter, LakeShore 325 temperature controller, test cell and computer.

3. RESULTS AND DISCUSSION

Figure 1 shows the XRD analysis of Mg:ZnO and MWCNTs/Mg:ZnO films. The x-ray patterns were corresponded with JCPDS card No.36-1451 and showed the polycrystalline pure hexagonal wurtzite structure of ZnO (Karaduman et.al., 2019). Three typical ZnO indexed peaks of (100), (002) and (101) were clearly observed (Sarf et.al., 2021). There was no purity peak such as metal, oxide, or any binary zinc alloy phases, or 'Mg' element peak or its compounds. A slightly shift was observed from (002) peak of ZnO seed layer and intensity of this peak can enhanced with Mg doping without changing wurtzite structure due to Mg^{2+} ionic radius (0.57 Å) which was so close Zn^{2+} ionic radius (0.60 Å). There was a very slight rolling of 26.16° and it has confirmed that the samples contained MWCNTs. The reason why there is no obvious characteristic C(002) peak in MWCNTs can be explained by the fact that dispersion is difficult in aqueous solutions and MWCNTs amount was so low and film growth process were too fast. In our prevous study which including ZnO/MWCNTs films, similar x-ray patterns of the unseen C (002) peak were obtained (Özütok et.al., 2019). Although preferential orientation of Mg:ZnO samples had high energy (002) peak along a-axis, MWCNTs/Mg:ZnO samples had low energy (101) preferential orientation peak along c-axis, indicating MWCNTs-ZnO matrix can change severly ZnO lattice parameters. In addition, it can be seen that the Mg element can settle in the ZnO host lattice and the coating of MWCNTs is relative succesfull in fast growth process.

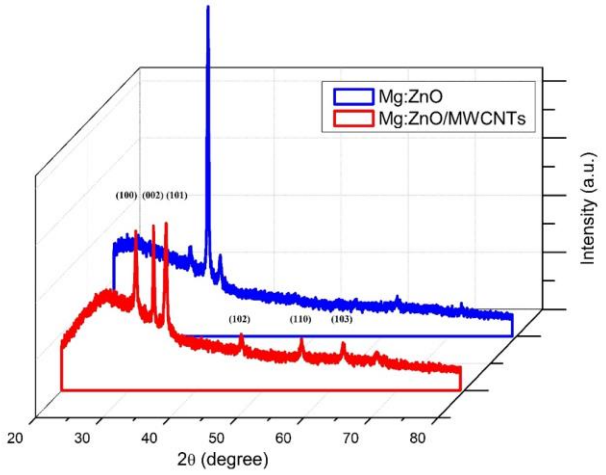

Figure 1. X-ray patterns of of Mg:ZnO and MWCNTs/Mg:ZnO films

.

Table 1. Structural parameters of Mg:ZnO and MWCNTs/Mg:ZnO films.

	Lattice parameters		**Aspect ratio (c/a)**	**Bond length 'L' (Å)**	**Crystallite size D (nm) From XRD**	**Dislocation density 'δ'**	**Strain 'ε' (x10^{-4})**	**APF**	**Volume of the nanoparticles**	**Volume of unit cell 'V' (Å)^3**	**No of unit cells**
	'a=b' (Å)	'c' (Å)									
Mg- doped ZnO	3.2236	5.1542	1.5988	1.9662	15	0.0044	24.40	0.7562	1767	46.38	38.09
MWCNTs coated Mg-doped ZnO	3.2163	5.1419	1.5987	1.9567	10	0.01	36.40	0.7563	523	46.06	11.35

Detailed structural parameters were listed in Table 1.

The values of lattice constants 'a' and 'c' are calculated by the following formula as shown by Equation (1) and (2) (Mia et.al., 2017);

$$a = \frac{\lambda}{\sqrt{3}\sin\theta} \quad (1)$$

$$c = \frac{\lambda}{\sin\theta} \quad (2)$$

'a' and 'c' values are compatible with the literature, as shown in Table 1 (Bilgili, 2021). The average crystallite size of the films are measured from X-ray line broadening of the preferential orientation peaks using Debye Scherrer's formula (Mujahid, 2015);

$$D = \frac{0.94\lambda}{\beta\cos\theta} \quad (3)$$

where, λ is the wavelength of x-ray radiation, β is the full width at half maximum (FWHM) and θ is diffraction angle. The average crystallite size of the films were estimated as 15 and 10 nm for Mg:ZnO and Mg:ZnO/MWCNTs films, indicating carbon nanotubes had an improving effect on the crystallinity due to high mechanical stability of tubes. Mujahıd et.al. reported that the average crystallite size of Pt-ZnO/CNT films were found from 14 nm to 24 nm. Umaralikhan et. al. calculated that the average crystallite size of Mg doped ZnO sample is 33 nm by using Debye-Scherrer's Formula (Umaralikhan et.al., 2017). Lattice strain formula is shown by Equation (4) (Sathya et.al, 2018);

$$\varepsilon = \frac{\beta\cos\theta}{4} \quad (4)$$

Due to low concentrated local impurity regions, increasing lattice strain with Mg doping and MWCNTs coating did not have a noticeable effect. A value associated with strain, dislocation density is calculated by Equation (5) (Mariappan et.al., 2014);

$$\delta=\frac{1}{D^2} \quad (5)$$

Dislocation density was relatively high in MWCNTs coated samples with decreasing crystalline size and increasing lattice strain. The following Equation (6) is used to calculate the volume of the unit cell for hexagonal system (Sathya et.al., 2018);

$$V=\frac{\sqrt{3}}{2}a^2c \quad (6)$$

The unit cell volumewas calculated by the above relation and were found to be 46.38 Å^3 and 46.06 Å^3 for Mg:ZnO and Mg:ZnO/MWCNTs samples, respectively. This indicated that Mg^{2+} ions and some C atoms that were difficult to separate reside partially in tetrahedral Zn^{2+} positions. Bond length is calculated by the relation as Equation (7) (Srinivasan et.al., 2007);

$$L=\sqrt{(\frac{a^2}{3}+(\frac{1}{2}-u)^2c^2)} \quad (7)$$

where a and c are lattice parameters, and u is defined as positional parameter of the wurtzite structure which is calculated by Equation (8) (Sathya et.al, 2018);

$$u=\frac{a^2}{3c^2}+0.25 \quad (8)$$

'u' parameter was 0.38 for both films. Bond length 1.9662 nm. and 1.9567 nm. for Mg:ZnO and Mg:ZnO/MWCNTs samples, respectively. These values were consistent with bulk zinc (1.97 nm.). APF was determined by Equation (9) (Bilgili et.al., 2021);

$$APF=\frac{2\pi a}{3\sqrt{3}c} \quad (9)$$

The APF of commercial ZnO was 74%. However, in our study, it was calculated about 75.6%. It can associate with that nanocrystals was slightly larger than that of bulk materials. The volume of the particles V is calculated from the equation and the volume of hexagonal unit cell has been estimated from ϑ. Then, the ratio (V/ ϑ) gives the number of unit cell present in a grain (Sathya et.al., 2018) ;

$$V=(\frac{4}{3})\pi((\frac{D}{2})^3) \quad (10)$$

$$\vartheta = 0.866a^2c \quad (11)$$

the volume of the particles were 1767 and 523, the volumes of hexagonal unit cell were 46.38 and 46.06 and the numbers of unit cell present in a grain are found 38.09 and 11.35 for Mg:ZnO and Mg:ZnO/MWCNTs films, respectively.

Figure 2 shows the SEM analysis of Mg doped ZnO and MWCNTs coated ZnO films. It could be highlighted from our previous study that, ZnO seed layer had nanoflower forms on the glass surface (Sarf et.al., 2020). With Mg doping, petal density of nanoflowers increased and relative nano-rod forms detect, indicating Mg doping can cause accumulation of petals during fast nucleation of ZnO and the rod froms and some observed agglomerative forms are thought to be associated with Mg assemblage. Dimension of nanoflowers of ~230 nm. increased with Mg doping. Wahyuono et.al. explained that the number of nucleation sites critically affects the self-assembly during nano-flower growth and the low concentration of OH- facilitates relatively high nucleation rates (Wahyuono et.al., 2016). Consistent nanoflower structures were observed in Mg:ZnO films as reported by Sagheer et.al. that explained by ZnO seed layer attribution and acts as the building block for the growth (Sagheer et.al., 2020). Lattice mismatch of ZnO seed layer and Mg doped layer may be also ensure its. When examinig the MWCNT effect, it was seen that it transformed

into relative heterogeneous (due to low solubility of nano-tubes in aqueous solution) nanowire-like structures onto nanoflower Mg:ZnO surfaces, induced pronounced wrinkling. Wrinkle formation is beneficial due to the pre-stress phase because it effectively reduces the intrinsic stress inside the film during functional stress and makes the films very suitable for opto-electronic devices such as touch screens (Liu et.al., 2021).

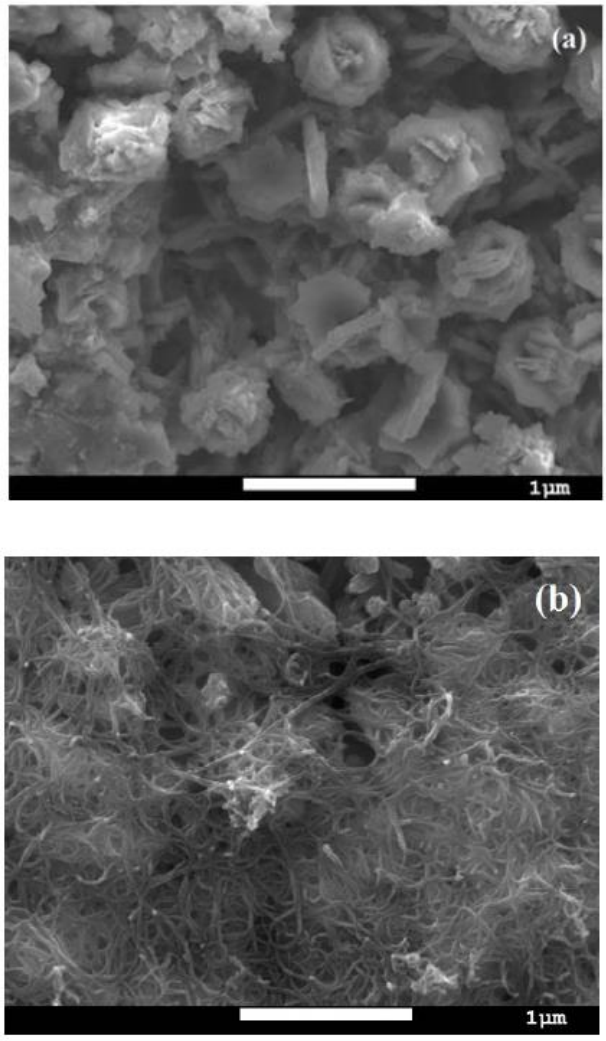

Figure 2. The SEM analysis of Mg:ZnO (a) and Mg:ZnO/MWCNTs films (b)

Uv-Vis absorption spectra of the samples as a function of the wavelength is shown in Figure 3 between 300-900 nm range. No impurity or defect related absorption was detected in the both films, indicating all films had high quality although fast grown of particles. Optical absorption edge at ~345 nm which was nearly similar for both films however MWCNTs coated samples had higher optical transparency which was a result of severe surface change with MWCNTs decoration and increasing homogeinity (Cwirzen et.al., 2008). The sharp absorption edge, which indicated a direct bandgap material, exhibited blue shifts with the increase of Mg content and MWCNTs coating. The phenomenon of absorption edge shifting to lower wavelength (as known blue shift) can be attributed to the Burstein-Moss effect and it is beneficial for optoelectronic applications due to a facilitation of phonon scattering from interfaces (Mohar et.al, 2020).

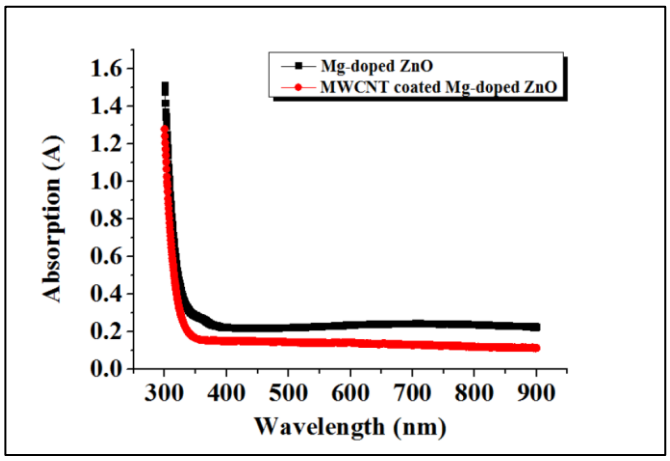

Figure 3. UV-Vis absorption spectra of Mg:ZnO and Mg:ZnO/MWCNTs films

Tauc relation was used for determining the optical direct bandgap, given by Equation (12) (Siregar et.al., 2020);

$$\alpha = \frac{A}{h\nu}\,(h\nu - E_g)^{1/2} \qquad (12)$$

where A is a constant, α is the absorption coefficient, E_g is the optical bandgap and hν is a photon energy. The optical band gap Eg of ZnO values were determined by the absorption spectra, as exhibited in Figure 4. Calculated Eg was 3.04 eV and 3.34 eV for Mg:ZnO and Mg: ZnO/ MWCNTs films, respectively. This increase indicated carbon nanotubes absorbed radiation in the Uv-Vis area, similar results was reported by Ramos-Corona et.al (Romas-Corona et.al., 2019).

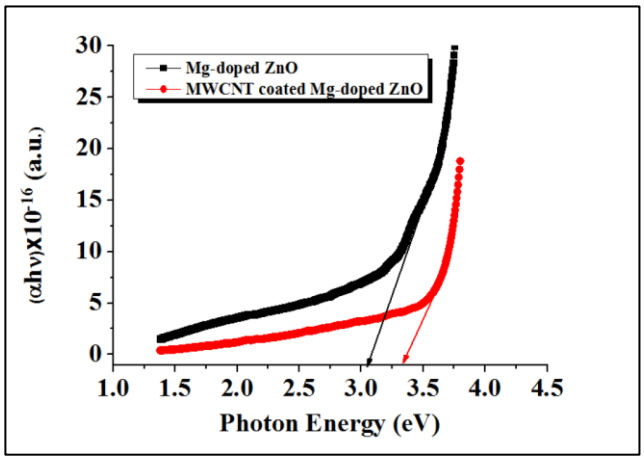

Figure 4. The optical band gap Eg of Mg:ZnO (a) and Mg:ZnO/MWCNTs films

Bandgap width and transition mechanisms were directly affected by the distribution of localized states in the bandgap which was known as the exponential Urbach tail. The Urbach tail of the films can be determined by the following relation (Ilican et.al., 2008);

$$\alpha = \alpha_o \exp\left(\frac{E}{E_U}\right) \qquad (13)$$

where E is the photon energy (hν), α_o is constant and E_U is the Urbach energy which refers the width of the exponential absorption edge. The E_U value was calculated from the slope of Equation (12) using relationship (14);

$$E_U = \left(\frac{d(\ln\alpha)}{d(h\vartheta)}\right)^{-1} \quad (14)$$

Eu values were calculated as 77 meV and 73 meV for Mg:ZnO and Mg:ZnO/ MWCNTs films. Urbach energy decrease indicated the decrease in the disorderliness of the film (Asikuzun et.al., 2018). The refractive index was calculated according to the five five different methods using band gap energies. According to the findings of Naccarato et. al., 2019, our material with (n > 2 and Eg > 3) considered in this research is classified as Transition Metals (TMs) with empty d shell (e.g. V^{5+}). Table 2 gives the refractive indexes that calculated by five different methods using band gap energies and detailed equations were revealed by Pattanaik et.al. (2020).

Table 2. Refractive index calculated by five different methods using band gap energies (Pattanaik, 2020).

Sample	Ravindra	Moss	Herve and Vandamme	Reddy and Anjayenulu	Kumar and Singh	Eg
Mg-doped ZnO	2.1868	2.3604	2.3102	2.7342	2.1240	3.06
MWCNTs coated Mg-doped ZnO	2.0132	2.3093	2.2333	2.6689	2.1815	3.44

Figure 5 represents FTIR spectrum of Mg:ZnO and Mg:ZnO/MWCNTs films to determine chemical composition of functional groups that was taken between 4000 cm^{-1} and 650 cm^{-1}. Typical OH^- group stretching vibration peak was observed around at 3746 cm^{-1} and 3392 cm^{-1} for Mg:ZnO and Mg:ZnO/MWCNTs films, indicating adsorbed water from film surface. The streching vibrations of carboxyl groups were detected at 2324 and 2343 cm^{-1} for Mg:ZnO and Mg:ZnO/MWCNTs samples. C-OH^- streching vibration related bands at ~1374 cm^{-1} were found in Mg:ZnO/MWCNTs samples (Srinet et.al., 2013). Asymmetric stretching of C=O bonds of the carboxylate ions were shown at 1396 cm^{-1} and 1374 cm^{1} in Mg:ZnO and Mg:ZnO/MWCNTs films. The peak at 865 cm^{-1} and 892 cm^{-1} are assigned to O-C-O stretching vibrations of the monodentate carbonate species (Etacheri et.al., 2012).

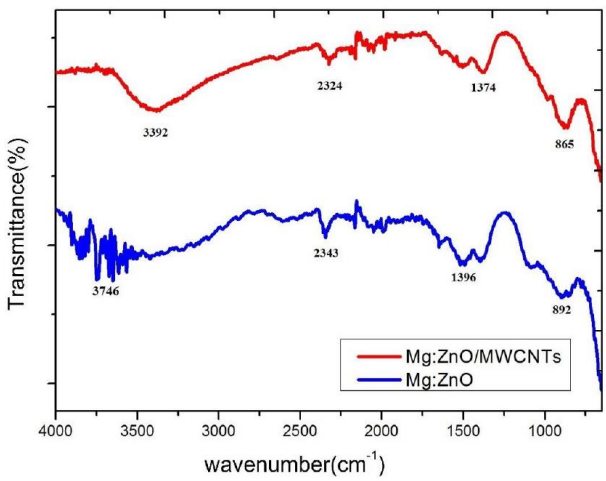

Figure 5. FTIR spectra of Mg:ZnO and Mg:ZnO/ MWCNTs films.

I-V characteristics of Mg:ZnO and Mg:ZnO/ MWCNTs films are shown in Figure 6 at room temperature. I-V characteristics were recorded with a sweep rate of 50 mV/s starting from +1 V to –1 V in a cycle at room temperature. These curves were not affected with the type of electrodes used (gold), and it was clear that, no non-linear behaviour was observed in the indicated voltage interval. The resistance of films at room temperature were calculated as 29.85 and 8.53 kΩ for Mg-doped ZnO and MWCNTs coated Mg-doped ZnO films, respectively (Kılınç et.al., 2010). Similarly, Chen et.al. has reported that the resistivity of the Mn doped ZnO increased with increasing Mn concentration (Chen et.al., 2007). Also, a decrease in resistance was observed with the MWNTS effect (Barthawala et.al., 2020). Particle size decrease could improve effect on the charge transfer and mobility. With MWCNTs coating, resistivity decrease was observed due to the presence of multi-walled carbon nanotubes in the samples produced a more significant number of charges (Diaz-Corona et.al. ,2019). In addition, the deviant of resistance values could be the result of the defect concentration by Mg-doping and MWCNT coating.

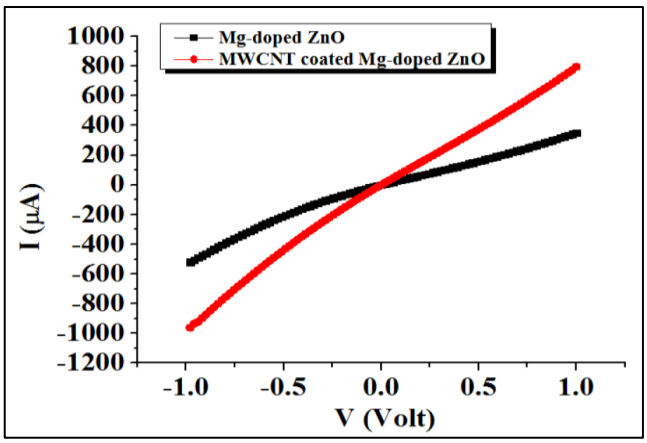

Figure 6. I-V characteristics of Mg:ZnO and Mg:ZnO/ MWCNTs films at room temperature.

4. CONCLUSIONS

The fabrication of Mg:ZnO with/without multi wall carbon nanotube (MWCNT) composite films and a study of their detailed structural analysis as well as optical and electrical properties have been reported. The nanocomposite films were deposited by ultra-fast (less than 10 minutes) chemical bath. The formation of the wurtzite-type hexagonal structure were observed in both of the ZnO and ZnO/MWCNTs composite thin films. Average crystallite size and crystal quality of the nanoflower ZnO seed layers exhibited noticeable improved change with Mg doping and MWCNTs coating. Electrical resistance of the samples decreased with

an increase was detected optical band gap by MWCNTs coating.

Ethics Committee Approval
N/A

Peer-review
Externally peer-reviewed.

Author Contributions
All authors have read and agreed to the published version of manuscript.

Conflict of Interest
The authors have no conflicts of interest to declare.

Funding
The authors declared that this study has received no financial support.

REFERENCES

Altun, B., Karaduman Er, I., Çağırtekin, A.O., Ajjaq A., Sarf, F., Acar, S. (2021). Effect of Cd dopant on structural, optical and CO_2 gas sensing properties of ZnO thin film sensors fabricated by chemical bath deposition method. Appl. Phys. A, 127**,** 687.

Asikuzun, E., Donmez, A., Arda, L., Cakiroglu, O., Ozturk, O., Akcan, D., Tosun, M., AtaoglU, S., Terzioglu, C. (2015). Structural and mechanical properties of (Co/Mg) co-doped nano ZnO Ceramic Inter. 41 6326.

Asikuzun, E., Ozturk, O., Arda, L., Terzioglu, C. (2017). Microstructural and electrical characterizations of transparent Er-doped ZnO nano-thin films prepared by sol-gel process J. Mater. Sci., Mater. Electron. 28, 14314–22.

Asikuzun, E., Ozturk, O., Arda, L., Terzioglu, C. (2018). Preparation, growth and characterization of nonvacuum Cu-doped ZnO thin films, Journal of Molecular Structure, 1165, 1-7.

Barthwala, S., Singh, N.B. (2020). Urea detection by ZnO-MWCNT nanocomposite sensor, Materials Today: Proceedings, 29;3, 749-752.

Bilgili, Ö. (2021). The structural and optical properties of Al and Mg doped ZnO synthesized by solid state reaction method, J. Baun Inst. Sci. Technol., 23(1), 50-64.

Chen, C. S., Xie, X. D., Liu, T. G., Lin, L. W., Kuang, J. C., Xie, X. L., Lu, L. J., Cao, S. Y. (2012). Multi-walled carbon nanotubes supported Cu-doped ZnO nanoparticles and their optical property, J Nanopart Res 14, 817.

Chen, W., Wang, J., Wang, M.R. (2007). Influence of doping concentration on the properties of ZnO:Mn thin films by sol–gel method, Vacuum 81, 894.

Cwirzen, A., Habermehl-Cwirzen, K., Penttala, V. (2008). No Access Surface decoration of carbon nanotubes and mechanical properties of cement/carbon nanotube composites, Advances in Cement Research, 20;2, 65-73.

Diaz-Corona, N., Martínez-Juárez, J., Pérez-Luna, J. G., Hernández-de la Luz, A. D., Rabanal, M. E., Robles-Águila, M. J. (2019). Structural, optical and electrical behavior of zinc oxide/ MWCNT composite thin films, Optical and Quantum Electronics, 51:220.

Edinger, S., Bansal, N., Bauch , M.,Wibowo, R.A., Hamid, R., Trimmel, G., Dimopoulos, T. (2017). Comparison of chemical bath-deposited ZnO films doped with Al, Ga and In. J Mater Sci., 52, 9410–9423.

Etacheri, V., Roshan, R., Kumar, V. (2012). Mg-doped ZnO nanoparticles for efficient sunlight-driven photocatalysis. ACS applied materials & interfaces.

Heiba, Z.K., Arda, L., Mohamed, M.B., Al-Jalali, M.A., Dogan, N. (2013). Structural and magnetic properties of (Al/Mg) Co-doped nano ZnO J. Supercond Nov. Magn 26 3299–304.

Ilican, S., Caglar, Y., Caglar, M., Yakuphanoglu, F. (2008). Structural, optical and electrical properties of F-doped ZnO nanorod semiconductor thin films deposited by sol–gel process, Applied Surface Science 255, 2353–2359.

Jaballah, S., Benamara, M., Dahman, H., A. Ly, D. Lahem , M. Debliquy, L. El Mir. (2020). Effect of Mg-doping ZnO nanoparticles on detection of low ethanol concentrations, Materials Chemistry and Physics, 255, 123643.

Kim, S., Nam, G., Yim, K.G. (2013). Effects of post-heated ZnO seed layers on structural and optical properties of ZnO nanostructures grown by hydrothermal method, Electron. Mater. Lett., 9, 293–298.

Majumder, S., Chatterjee, S., Basnet, P., Mukherjee, J. (2020). ZnO based nanomaterials for photocatalytic degradation of aqueous pharmaceutical waste solutions – A contemporary review, Environmental Nanotechnology, Monitoring & Management, 14, 100386.

Karaduman E. I., Nurtayeva, T., Sbeta, M., Cagirtekin, A. O., Acar, S., Yildiz,A. (2019). Carbon monoxide gas sensing performance of ZnO:Al thin films prepared using different solvent–stabilizer combinations. J Mater Sci: Mater Electron., 30, 10560–10570.

Kılınç, N., Arda, L., Öztürk, S., Öztürk, Z. Z. (2010). Structure and electrical properties of Mg-doped ZnO nanoparticles, Cryst. Res. Technol. 45; 5, 529 – 538.

Kumar V. A., Lee, W.-J., Chung., Y.-D., Kim, J. (2021). Growth and device properties of ALD deposited ZnO films for CIGS solar cells, Materials Science in Semiconductor Processing, 121, 105406.

Liu, S., Zhu, L., Cao, W., Li, P., Zhan, Z., Chen , Z., Yuan, X., Wang, J. (2021). Defect-related optical properties of Mg-doped ZnO nanoparticles synthesized via low temperature hydrothermal method, Journal of Alloys and Compounds 858, 157654.

Mariappan, R., Ponnuswamy, V., Chandra A. Bose, Chithambararaj, A., Suresh, R., Ragavendar, M. (2014). Structural, optical and electrical characterization of nebulizer sprayed ZnO nano-rods. Superlattices Microstruct., 65, 184–94.

Mia, M.N.H., Pervez, M.F., Khalid Hossain, M., Reefaz M. Rahman, Jalal Uddin, M., Al Mashud, M.A., Ghosh, H.K., Hoq, M. (2017). Influence of Mg content on tailoring optical bandgap of Mg-doped ZnO thin film prepared by sol-gel method, Results in Physics. 7, 2683–2691.

Mujahıd, M. (2015). Synthesis, characterization and electrical properties of visible-light-driven Pt-ZnO/CNT, Bull. Mater. Sci., 38;4, 995–1001.

Mohar, R.S., Sugihartono, I., Fauzia, V., Umar, A.A. (2020). Dependence of optical properties of Mg-doped ZnO nanorods on Al dopant, Surfaces and Interfaces, 19, 100518.

Naccarato, F., Ricci, F., Suntivich, J., Hautier, G., Wirtz, L., Rignanese, G.-M. (2019). Searching for materials with high refractive index and wide band gap: A first-principles high-throughput study, Phys. Rev. Materials 3, 044602.

Okeke, I.S., Agwu, K.K., Ubachukwu, A.A., Madiba, I.G., Maaza, M., Whyte, G.M., Ezema, F. I. (2021). Impact of particle size and surface defects on antibacterial and photocatalytic activities of undoped and Mg-doped ZnO nanoparticles, biosynthesized using one-step simple process, Vacuum, 187, 110110.

Özütok, F., Karaduman E.I., Acar, S., Demiri, S. (2019). Enhancing the CO gas sensing properties of ZnO thin films with the decoration of MWCNTs. J Mater Sci: Mater Electron., 30, 259–265.

Pattanaik, A., Tripathy, S.K., Naik, P., Meher, D.K. (2021). Structural and elastic properties of binary semiconductors from energy gaps, Applied Physics A, 127, 14.

Popielarski, P., Mosinska, L., Bala, W., Paprocki, K., Yu Zorenko, Zorenko, T., Sypniewska, M. (2019). Persistent photoconductivity in ZnO thin films grown on Si substrate by spin coating method, Optical Materials, 97, 109343.

Ramos-Corona, A., Rangela, R., Alvarado-Gil, J.J., Bartolo-Pérez, P., Quintana, P., Rodríguez-Gattorno, G. (2019). Photocatalytic performance of nitrogen doped ZnO structures supported on graphene oxide for MB degradation, Chemosphere, 236, 124368.

Rodnyi, P.A., Khodyuk, I.V. (2011). Optical and luminescence properties of zinc oxide Opt. Spectrosc. 111 776–85.

Sarf, F., Karaduman I. E., Yakar, E., Acar, S. (2020). The role of rare-earth metal (Y, Ru and Cs)-doped ZnO thin films in NH_3 gas sensing performances at room temperature, Journal of Materials Science: Materials in Electronics 31, 10084–10095.

Sarf, F., Kızıl, H. (2021). Defect Emission Energy and Particle Size Effects in Fe:ZnO Nanospheres Used in Li-Ion Batteries as Anode. *J. Electron. Mater.* 50**,** 6475–6481.

Srinet, G., Kumar, R., Sajal., V. (2013). Effects of Mg doping on the structural and optical properties of ZnO nanoparticles, AIP Conference Proceedings 1536, 247.

Sathya, M., Pushpanathan, K. (2018). Synthesis and Optical Properties of Pb Doped ZnO Nanoparticles, Applied Surface Science, 449, 346–357.

Srinivasan, G., Rajendra Kumar, R.T., Kumar, J. (2007). Li doped and undoped ZnO nanocrystalline thin films: a comparative study of structural and optical properties. J Sol-Gel Sci Technol, 43, 171–7.

Sahoo, T., Jang, LW., Jeon, DW., Yu, Y.-T., Lee, I.-H. (2013). Hydrothermal growth of single crystal ZnO nanorods on surface-modified graphite. Electron. Mater. Lett., 9, 715–718.

Samadi, M., Zirak, M., Naseri, A., Khorashadizade E., Moshfegh A. Z. (2016). Recent progress on doped ZnO nanostructures for visible-light photocatalysis, Thin Solid Films, 605, 2–19.

Sagheer, R., Khalil, M., Abbas, V., Kayani, Z.N., Tariq, U., Ashraf, F. (2020). Effect of Mg doping on structural, morphological, optical and thermal properties of ZnO nanoparticles, Optik - International Journal for Light and Electron Optics 200, 163428.

Sharma, S., Periasamy, C., Chakrabarti, P. (2015). Thickness dependent study of RF sputtered ZnO thin films for optoelectronic device applications. Electron. Mater. Lett., 11, 1093–1101.

Senol, S.D., Yalcin, B., Ozugurlu, E., Arda, L. (2020). Structure, microstructure, optical and photocatalytic properties of Mn-doped ZnO nanoparticles, Mater. Res. Express 7, 015079.

Siregar, N., M. dan Johnny Panggabean (2020). The effect magnesium (Mg) on structural and optical properties of ZnO:Mg thin film by sol-gel spin coating method, Journal of Physics: Conference Series 1428, 012026.

Tan, C., Sun, D., Xu, D., Tian, X., Huang, Y. (2016). Tuning electronic structure and optical properties of ZnO monolayer by Cd doping. Ceramics International, 42, 10997–11002.

Umaralikhan, L., Mohamed Jaffar, M.J. (2017). Green synthesis of ZnO and Mg doped ZnO nanoparticles, and its optical properties, J Mater Sci: Mater Electron., 28, 7677–7685.

Üzar, N., Algün, G., Akçay, N., Akcan, D., Arda, L. (2017). Structural, optical, electrical and humidity sensing properties of (Y/Al) co-doped ZnO thin films J. Mater. Sci., Mater. Electron. 28, 11861–70.

Yang, Y., Wang, J., Li, X., Lang, J., Liu, F., Yang, L., Zhai, H., Gao, M., Zhao, X. (2012). Effect of polar and non-polar surfaces of ZnO nanostructures on photocatalytic properties, Journal of Alloys and Compounds, 528 28–33.

Yao, M., Ding, F., Cao, Y., Hu, P., Fan, J., Lu, C., Yuan, F., Shi, C., Chen, Y. (2014). Sn doped ZnO layered porous nanocrystals with hierarchical structures and modified surfaces for gas sensors, Sensors and Actuators B, 201, 255–265.

Wahyuono, R.A., Schmidt, C., Dellith, A., Dellith, J., Schulz, M., Seyring, M., Rettenmayr, M., Plentz, J., Dietzek, B. (2016). ZnO nanoflowers-based photoanodes: Aqueous chemical synthesis, microstructure and optical properties. Open Chem., 14:158-169.